Multi-Diffusion Domain Modeling of Meteorite $^{40}Ar/^{39}Ar$ Data

By:
Evan S. Tucker
Department of Geological Sciences, University of Colorado Boulder

Defended: April 5, 2019

Thesis Advisor:
Dr. Carolyn A. Crow, Department of Geological Sciences

Defense Committee:
Dr. Carolyn A. Crow, Department of Geological Sciences
Prof. Brian M. Hynek, Department of Geological Sciences
Prof. Ann-Marie Madigan, Department of Astrophysical & Planetary Sciences

Abstract

The majority of $^{40}Ar/^{39}Ar$ analyses involving extraterrestrial samples were collected from bulk rock samples due to fine grain sizes. This present challenges in modeling the diffusion kinetics and thermal histories of these samples because of the presence of multiple-diffusion domains. Since Lovera et al. (1989) developed the multi-diffusion domain (MDD) method of modeling, many attempts have been made to automate the modeling process. However, existing software to model diffusion parameters and thermal histories falls short in that it is either restricted in availability, restricted in flexibility, or is cumbersome to use. I have created a new program, OPTIMuM (Optimize Parameters To Interpret Multiple Minerals), that models bulk samlpe diffusion kinetics and thermal histories through a simple graphical user interface (GUI). In this paper, I present the theory behind OPTIMuM as well as modeling results of samples from three extraterrestrial bodies. These results have important implications for the impact history and the dynamical evolution of the early solar system.

Contents

List of Figures

List of Tables

Acknowledgements

I would first like to thank my advisor and mentor Dr. Carolyn Crow. She has gone above and beyond in every way, helping me complete this project, write proposals, and present my work. Carolyn was always eager to meet to discuss the project, even if we spent an hour hunting down a typo in the code. Thank you to Prof. Brian Hynek for his assistance in navigating the honors thesis process and being a part of my committee. I would also like to thank Prof. Ann-Marie Madigan for bringing her perspective to the committee. Finally, I want to thank UROP, PACE, and the Geology Department for funding various parts of this project and helping me present my work along the way.

1 Introduction

The early impact history of the solar system is important for understanding its dynamical evolution, which gives insights into outstanding questions in planetary science such as the timing of giant planet migration and delivery method of water to Earth. The oldest terrestrial rock samples date to about 4 Ga (Bell et. al., 2014) due to plate tectonics and weathering process that continually resurface the Earth and inhibit preservation of ancient crustal rocks. These processes do not affect the Moon or meteorite parent bodies (except for Mars), thus these samples provide the only direct means to constrain the timing and nature of early impacts. Isotopic dating methods such as K–Ar and $^{40}Ar/^{39}Ar$ have been applied to multiple extraterrestrial samples and have historically been used to constrain the ages of impact events across the solar system. However, many of these impact ages have been called into question because $^{40}Ar/^{39}Ar$ data has relied on interpretation by individual researchers and this system is susceptible to thermal resetting (e.g. Boehnke & Harrison, 2016). Swindle, Kring, & Weirich (2014) discuss other difficulties involving $^{40}Ar/^{39}Ar$ analysis of extraterrestrial samples, which include small grain sizes in these samples and complex diffusion kinetics arising from the necessity to conduct whole rock analyses. There are additional complications from extraneous Ar within the samples from processes such as solar wind implantation and irradiation by high energy particles on the surface of parent bodies or during transit to Earth. However, most of these effects are either correctable or able to provide valuable information if effort is made to understand the complexities in the data.

For example, partial resetting of extraterrestrial samples is often interpreted as heating from an impact event. Over 100 $^{40}Ar/^{39}Ar$ ages of ordinary chondrites have been determined (Swindle et al., 2014), and many of the age spectra show evidence of partial resetting making it difficult to interpret the significance of the ages from the age spectra alone. However, the benefit of the $^{40}Ar/^{39}Ar$ method is that through modeling the diffusion kinetics in the sample, the thermal history can be constrained, which allows for the timing and temperature of the heating events (e.g. impacts) to be understood (Turner, 1968). For single mineral samples,

this type of thermal modeling is relatively straightforward, but the majority of published extraterrestrial $^{40}Ar/^{39}Ar$ data were analyzed as bulk samples due to fine grain size. This means that multiple mineral phases are present and the thermal modeling becomes non-trivial since each phase has its own diffusion parameters and gas amounts, which must be determined by inverse modeling. As such, this type of modeling has not been widely applied to $^{40}Ar/^{39}Ar$ thermochronology data sets, especially for the extraterrestrial samples. The goals of this project are to (1) create user-friendly software to model diffusion kinetics and thermal histories of samples with multiple diffusion domains (MDD) and (2) apply MDD modeling to historical meteorite $^{40}Ar/^{39}Ar$ data to investigate thermal histories of asteroid parent bodies.

2 Background

2.1 *Overview of the $^{40}Ar/^{39}Ar$ Method*

The $^{40}Ar/^{39}Ar$ dating method arose from the K–Ar method (McDougall & Harrison, 1999; Lovera, Richter, & Harrison, 1989) and has nearly replaced K–Ar entirely in modern analyses. Both methods rely on K decaying to Ar: $^{40}K \longrightarrow {}^{40}Ar$, but the $^{40}Ar/^{39}Ar$ method takes advantage of the thermal neutron induced reaction: $^{39}_{19}K + {}^{1}_{0}n \longrightarrow {}^{1}_{1}p + {}^{39}_{18}Ar$, to infer the amount of K in the sample (McDougall & Harrison, 1999). This simplifies the laboratory process since only a single mass spectrometer is required to measure all relevant Ar isotopes. The sample age is then determined from the $^{40}Ar^*/^{39}Ar_K$, where $^{40}Ar^*$ is the radiogenic Ar and $^{39}Ar_K$ is the K derived ^{39}Ar from the laboratory. Table 1 summarizes the different notation and constant values used in this paper. In nature, the $^{39}K/^{40}K$ ratio is constant, which means the $^{40}Ar^*/^{39}Ar_K$ can be used to compute the age since it is proportional to $^{40}Ar^*/^{40}K$ and $^{39}Ar_K$ is derived directly from ^{39}K (McDougall & Harrison, 1999). For extraterrestrial samples, this method is particularly favorable as each analysis needs only a small amount of sample (Merrihue & Turner, 1966).

2.2 *Diffusion Theory & Fractional Loss*

Here I will briefly discuss the basis of diffusion theory, which governs Ar movement and distribution within sample grains. I reproduce several important equations given in McDougall & Harrison (1999), who derive these equations in more detail. Fourier's Law of Heat Conduction states

$$\frac{q}{A_x} = F = -K\frac{\partial T}{\partial x} \tag{1}$$

where q is the heat transfer rate, A_x is cross-sectional area, F is the flux of heat across the surface, K is thermal conductivity, and T is temperature. Fick's First Law extends (1) to mass such that

$$\frac{q}{A_x} = F = -D\frac{\partial C}{\partial x} \tag{2}$$

where D is known as the diffusion coefficient and C is the concentration. Through three dimensional conservation of energy, it can be shown that

$$\frac{\partial^2 T}{\partial x^2} + \frac{\partial^2 T}{\partial y^2} + \frac{\partial^2 T}{\partial z^2} + \frac{Q}{K} = \frac{1}{\kappa}\frac{\partial T}{\partial t} \tag{3}$$

with thermal diffusivity $\kappa = K/(c_p\rho)$, ρ equal to density, and c_p equal to heat capacity. (3) extends to molecular diffusivity according to Fick's Second Law:

$$\frac{\partial C}{\partial t} = D\left(\frac{\partial^2 C}{\partial x^2} + \frac{\partial^2 C}{\partial y^2} + \frac{\partial^2 C}{\partial z^2}\right) \tag{4}$$

(4) is geometry dependent and can be solved to find D. While there are several crystal geometries, I consider only spherical and plane sheet, which have respective one-dimensional solutions of

$$C = \frac{C_0 2r}{\pi R}\sum_{n=1}^{\infty}\frac{(-1)^n}{n}\sin\left(\frac{n\pi R}{r}\right)\exp\left(\frac{-n^2\pi^2 Dt}{r^2}\right) \tag{5}$$

$$C = \frac{4C_0}{\pi}\sum_{n=1}^{\infty}\frac{(-1)^n}{2n+1}\exp\left(\frac{-D(2n+1)^2\pi^2 t}{4r^2}\right)\cos\left(\frac{(2n+1)\pi R}{2r}\right) \tag{6}$$

Table 1: Notations and constants used in this study.

Isotope/Parameter	Description
^{40}Ar*	Trapped radiogenic Ar from ^{40}K decay
$^{40}\mathrm{Ar}_{\mathrm{out}}$	Amount of ^{40}Ar at time of thermal event
$^{40}\mathrm{Ar}_{2}$	Amount of ^{40}Ar formed after thermal event
$^{40}\mathrm{Ar}_{\mathrm{pres}}$	Amount of ^{40}Ar presently observed
$^{39}\mathrm{Ar}_{\mathrm{K}}$	K derived Ar from laboratory irradiation
q	Heat transfer rate
A_{x}	Cross-sectional area
F	Flux of heat (for equations (1) and (2) only)
K	Thermal conductivity
T	Temperature
T_{max}	Maximum temperature during thermal event
α	Cooling rate parameter that incorporates surface area and emissivity
D	Diffusion coefficient
C	Concentration of diffusant
κ	Thermal diffusivity
c_p	Specific heat
ρ	Density
t	Time
t_{age}	Sample age
t_c	Crystallization age
t_{out}	Outgassing age
r	Sphere radius or half-sheet thickness
R	Diffusant position within a grain
f	Cumulative fractional release of ^{39}Ar, unless another isotope is specified
F	Fraction of Ar within a mineral phase, isotope specified by subscript
$f(x)$	Total fractional loss from thermal event
J	Irradiation parameter
E_a	Activation energy
R	Boltzmann gas constant, 8.314 $J/(mol \cdot K)$
λ_{40K}	^{40}K decay constant, 5.543×10^{-10} (Steiger & Jäger, 1977)

where r is radius or half-sheet thickness, and R is position within the grain. (5) and (6) thus describe the distribution of a diffusant in the respective geometry.

While it is impractical to solve for D, the quantity Dt/r^2 will prove useful as it is related to the fractional loss of diffusant from system, which we can more readily measure. This measurement comes from heating in the laboratory, which I discuss in the next section. The fractional loss f of a sphere ((7) & (8)) and plane sheet ((9) & (10)) for a given time t are approximated from infinite sums as

$$f \approx 1 - \left(\frac{6}{\pi^2}\right) \exp\left(\frac{-\pi^2 Dt}{r^2}\right) \qquad 0.85 \leq f \leq 1 \tag{7}$$

$$f \approx \left(\frac{6}{\pi^{3/2}}\right) \left(\frac{\pi^2 Dt}{r^2}\right)^{1/2} - \left(\frac{3}{\pi^2}\right) \left(\frac{\pi^2 Dt}{r^2}\right) \qquad 0 \leq f \leq 0.85 \tag{8}$$

$$f \approx 1 - \left(\frac{8}{\pi^2}\right) \exp\left(\frac{-\pi^2 Dt}{4r^2}\right) \qquad 0.45 \leq f \leq 1 \tag{9}$$

$$f \approx \left(\frac{2}{\sqrt{\pi}}\right) \left(\frac{Dt}{r^2}\right)^{1/2} \qquad 0 \leq f \leq 0.6 \tag{10}$$

and come from integration of equations (5) and (6). Figure 1 shows the relationship between f and Dt/r^2 for four different geometries.

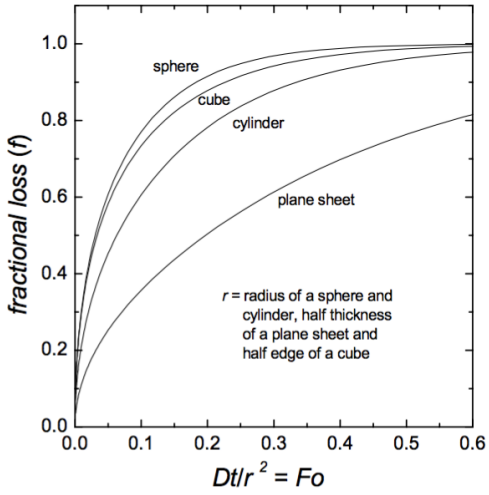

Figure 1: Relationship between f and Dt/r^2 for four different geometries, digitally reproduced from Harrison & Zeitler (2005), originally in McDougall & Harrison (1999).

2.3 *The Age Equation, Step Heating Experiments, & The Arrhenius Relationship*

Merrihue & Turner (1966) published the first $^{40}Ar/^{39}Ar$ step heating analyses where the sample is outgassed at progressively increasing temperatures for a given duration. This method provides relative ages at each step that can be plotted as an age spectra and provide information on Ar distribution in the sample (figure 2). Of particular interest is the fact that the step heating method allows one to identify excess or lost $^{40}Ar^*$ based on the $^{40}Ar^*/^{39}Ar_K$ of each step (figure 2).

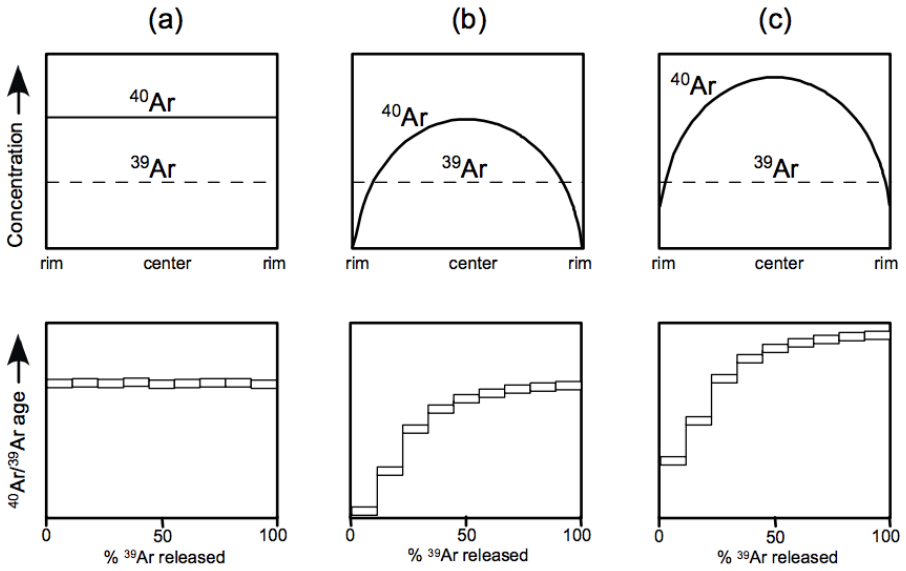

Figure 2: Schematic displays of Ar distribution in ideal minerals (top) and the resulting age spectra (bottom). a) undisturbed mineral from crystallization that produces a flat age spectra; b) partial loss of $^{40}Ar^*$ in geologically recent times; c) the same as b) except $^{40}Ar^*$ has accumulated since the loss event. Digitally reproduced from Harrison & Zeitler (2005), originally in McDougall & Harrison (1999).

It is worth briefly describing the laboratory procedures used in $^{40}Ar/^{39}Ar$ dating as it will relate equations (7)–(10) to the modeling process. Prior to outgassing, the sample is irradiated along with a standard of known K–Ar age with fast neutrons to convert ^{39}K to ^{39}Ar (Harrison & Zeitler, 2005). The known standard is used to monitor the neutron flux during irradiation such that the age of the sample can then be determined (Harrison & Zeitler, 2005). I will derive the age equation used in $^{40}Ar/^{39}Ar$ analyses, and it is covered in greater detail in McDougall & Harrison (1999). A given amount of radioactive substance N

at time t will undergo decay with proportionality constant λ such that

$$\frac{dN}{dt} = -\lambda N \tag{11}$$

which can be integrated to obtain the amount of parent N at any time t

$$N = N_0 \exp(-\lambda t) \tag{12}$$

where N_0 is the amount of parent initially at $t = t_0$. Since N_0 equals the sum of N and amount of daughter D at a given time, equation (12) can be modified and rearranged to show the general age equation.

$$t = \frac{1}{\lambda} \ln \left(1 + \frac{D}{N} \right) \tag{13}$$

This equation can again be modified to calculate ages for the ^{40}Ar/^{39}Ar system. Due to the dual decay of ^{40}K to ^{40}Ca and ^{40}Ar, a substitution must be made for the fraction of the ^{40}K decay constant λ_{40K} that produces ^{40}Ar such that

$$t = \frac{1}{\lambda_{40K}} \ln \left(1 + \frac{\lambda_{40K}}{\lambda_e + \lambda'_e} \frac{^{40}Ar*}{^{40}K} \right) \tag{14}$$

which is then rearranged to obtain

$$^{40}Ar* = {}^{40}K \frac{\lambda_e + \lambda'_e}{\lambda_{40K}} (\exp(\lambda_{40K} t) - 1) \tag{15}$$

Additionally, the amount of $^{39}\mathrm{Ar_K}$ produced during laboratory irradiation time Δ with neutron flux and neutron capture cross section at energy E, $\phi(E)$ and $\sigma(E)$, can be calculated as shown in (16).

$$^{39}Ar_K = {}^{39}K \Delta \int \phi(E) \sigma(E) dE \tag{16}$$

Finally, we ratio (15) and (16) to find

$$\frac{^{40}Ar*}{^{39}Ar_K} = \frac{^{40}K}{^{39}K} \frac{\lambda_e + \lambda'_e}{\lambda_{40K}} \frac{1}{\Delta} \frac{\exp(\lambda_{40K} t) - 1}{\int \phi(E) \sigma(E) dE} \tag{17}$$

Conventionally, the irradiation parameter J is defined as

$$J = \frac{^{39}K}{^{40}K}\frac{\lambda_{40K}}{\lambda_e + \lambda'_e}\Delta \int \phi(E)\sigma(E)dE \tag{18}$$

which is then substituted in to (17) and rearranged for age t.

$$t_{age} = \frac{1}{\lambda_{40K}} \ln\left(1 + J\frac{^{40}Ar*}{^{39}Ar_{\mathrm{K}}}\right) \tag{19}$$

As it is impractical to solve for J using equation (18), a standard of known age is irradiated with the sample to monitor the dose of neutrons. From the standard, J can be calculated as shown in (20).

$$J = \left(\frac{^{39}Ar_K}{^{40}Ar*}\right)\left(\exp^{\lambda_{40K}t} - 1\right) \tag{20}$$

Since the age of standard is well known and its Ar content can be measured with the unknown, (20) is combined with (19) to calculate the age of the sample at each step in the laboratory heating schedule. Note that this shows another advantage of the ^{40}Ar/^{39}Ar method because one need not measure absolute abundances of isotopes and can instead compute an age from relative abundances.

In the step heating method, samples are heated at increasing temperature, for a typically uniform duration, and Ar isotope abundances are measured. Given a laboratory heating schedule (i.e. temperature and time) and fraction of ^{39}Ar released in each step, we can calculate the diffusion coefficient of each step by rearranging equations (7)–(10). It should be noted that normalizing the diffusion coefficient to r^2 allows us to calculate the diffusion kinetics for multiple phases without having to know the grain or domain size. Diffusion kinetics modeling is based on the ^{39}Ar data since it was produced in a reactor and has not been disturbed before laboratory outgassing.

The Arrhenius equation (21) describes the relationship between D/r^2, the activation energy E_a, and the pre-exponential factor D_0/r^2,

$$\ln\left(\frac{D}{r^2}\right) = -\left(\frac{E_a}{2.303RT}\right) + \ln\left(\frac{D_0}{r^2}\right) \tag{21}$$

with R equal to the Boltzmann gas constant. Figure 3 shows an Arrhenius plot, which represents this relationship graphically. To create an Arrhenius plot for a sample, we can use the fraction of ^{39}Ar released (f) in each laboratory heating step to calculate D/r^2 using (7)–(10). The natural log of the D/r^2 values are then plotted against $1/T$. In the case of a single diffusing phase, the data should define a line. In the case of multiple domains, the Arrhenius plot will be more complicated and non-linear.

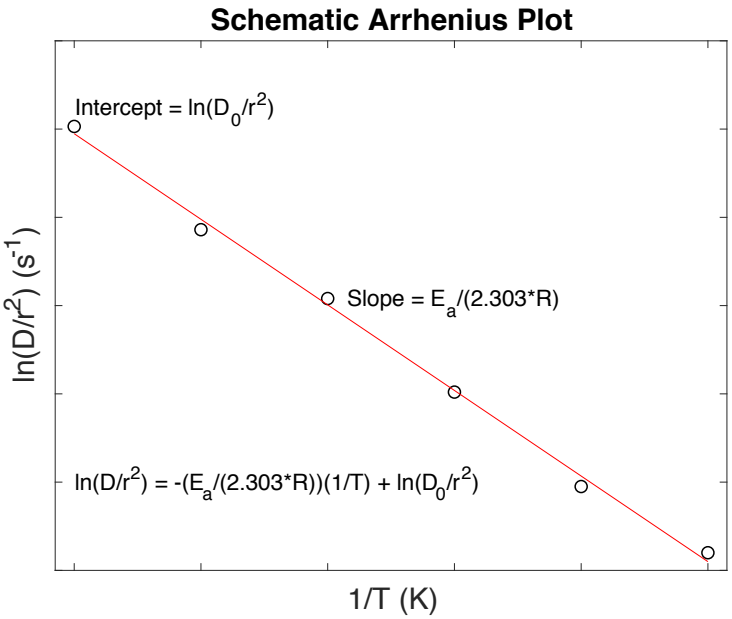

Figure 3: Schematic Arrhenius plot (generated from an artificial dataset). Note the inverse temperature and the relationships to equation (21).

2.4 *The Multi-Diffusion Domain Method & Model*

For fine-grained samples, including many extraterrestrial ones, mineral separation is too difficult and bulk analysis is performed instead. Lovera et al. (1989) developed the MDD method to understand the diffusion parameters and cooling histories of whole rock or multi-domain samples.

On an Arrhenius plot, modeled diffusion domains can be represented as lines (figure 4). The total gas released from a bulk rock sample is the sum of the gas released from each phase. This is reflected on the Arrhenius plot, where the data on the right side of the plot falls between two lines, indicating that it is a mixture of gas from multiple phases. On the

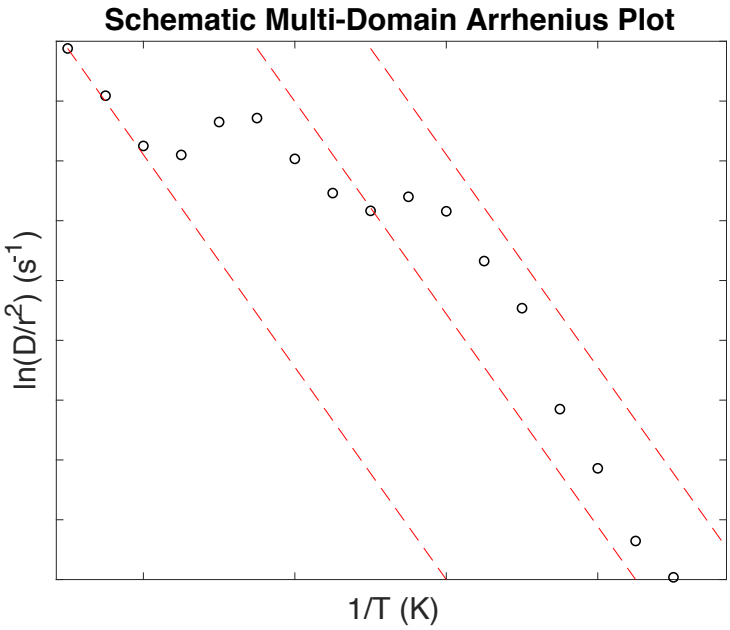

Figure 4: Schematic Arrhenius plot for a sample with multiple domains (generated from an artificial dataset). Each diffusion domain is represented as a dashed line.

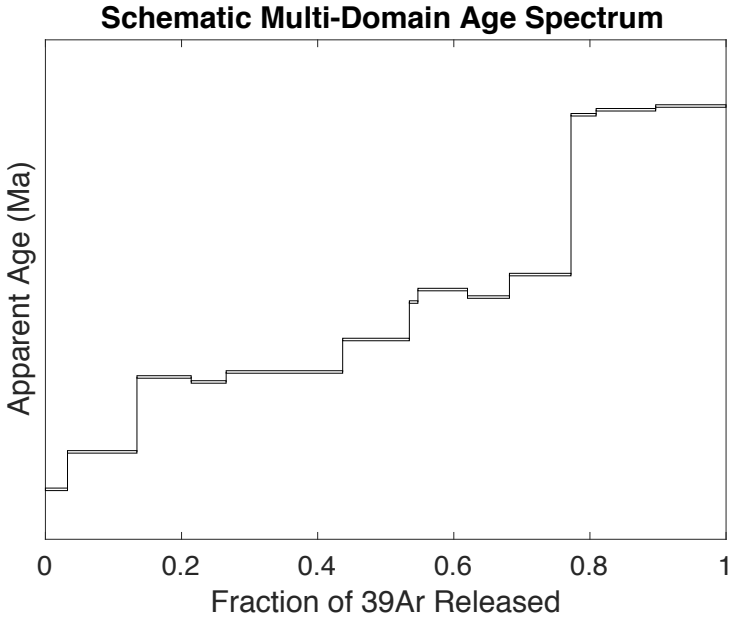

Figure 5: Schematic age spectra for a sample with multiple domains (generated from an artificial dataset). The widths of the boxes are the cumulative fraction of gas released in each laboratory step, and the heights are the uncertainties in the apparent ages.

left side of the plot, the data lie on a line, which shows gas release from only one phase. Each phase will contain some fraction of the total ^{39}Ar released in the lab, F_{39}, and some fraction of the total ^{40}Ar released in the lab, F_{40}, which are not necessarily the same. The goal of my diffusion kinetics modeling is to constrain the following four parameters for each phase: E_a, D_0/r^2, F_{39}, and F_{40}.

For one phase samples, where the Arrhenius plot is linear, the E_a is proportional to the slope of the line and the $\ln(D_0/r^2)$ is equal to the intercept; F_{39} and F_{40} are assumed to be one since all the gas resides in one phase. However, the Arrhenius plot becomes non-linear with multi-phase samples and an optimization routine is necessary to determine the number of phases, the associated diffusion kinetics, and the distribution of gas within the sample. While there does exist MDD modeling software (e.g. Lovera, 1992), it is either restricted in availability, requires significant user input, or is restricted in the type and mixture of phases that can be used. My program, OPTIMuM, is written in MATLAB and has a user-friendly design in a graphical user interface (GUI); it also allows for more flexibility in terms of sample mineralogy and optimization options. In the following sections, I will present the software design as well as a suite of results of thermal modeling for ^{40}Ar/^{39}Ar data from lunar, Martian, and chondritic samples.

3 Methods

3.1 *Diffusion Kinetics Modeling*

I started by writing a modular program to model samples with one mineral phase. Laboratory data is first saved in an Excel spreadsheet according to the template shown in Appendix A. Both the one phase program and OPTIMuM assume that the user has made all necessary corrections to the data (e.g. atmospheric and cosmic ray corrections). Multiple samples can be put in one Excel document, however, each sample needs to be on a separate sheet. The user has the ability to select the sheet with the desired data in the GUI. The one phase program used a least squares linear regression to fit E_a and D_0/r^2 since the hypothetical Arrhenius plot for a single-phase system is linear. To fit these two parameters, we

first need to generate an Arrhenius plot from the laboratory data to find $\ln(D_0/r^2)$ of each step from the f of the data. A best fit line is then calculated with the slope related to E_a and the intercept related to $\ln(D_0/r^2)$ by (21). The program then determines the modeled $^{40}Ar/^{39}Ar$ age spectrum that would result from the E_a, $\ln(D_0/r^2)$, F_{39}, and F_{40} (here both are equal to one). This is done in four steps: (1) the E_a and $\ln(D_0/r^2)$ are used to determine the D/r^2 for each laboratory heating step; (2) the fraction of gas loss (f) is calculated using equations (7)–(10) depending on the assumed geometry; (3) the F_{39} and F_{40} are multiplied by the f of each step to determine the ^{39}Ar and ^{40}Ar released in each step; and (4) the age of each step is determined from the $^{40}Ar/^{39}Ar$ ratio using equation (19). The program does one final modeling step, which is to produce an Arrhenius plot from the modeled age spectra. Comparison between the measured and modeled Arrhenius plot allows us to determine how well our E_a and $\ln(D_0/r^2)$ represent the actual diffusion kinetics of the sample. This is not so important for the single phase sample, but is very useful for multi-phase samples. Writing the one-phase code in this way made the transition to the multi-phase code simpler.

The multi-phase optimization program, OPTIMuM, expands on the one phase code with several key differences to incorporate the MDD method. Figure 6 shows the general programmatic flow of OPTIMuM. It is run through a GUI in MATLAB to simplify the optimization process for the end-user, who can easily import data, select the correct sheet, enter a J value, and choose a geometry. Importantly, OPTIMuM adds two additional parameters to fit: F_{39} and F_{40}, which are no longer equal to one in the presence of multiple phases. The modeling steps in OPTIMuM are the same as the one phase program, except that the Arrhenius plot is not fit with a line. Instead, the user inputs an initial guess for the number of phases and the type of phases either manually or from preset values of plagioclase and pyroxene (Cassata, Renne, & Shuster, 2009 & 2011). The program then assumes a randomly generated initial guess for F_{39} and F_{40} of each phase, and the fraction of gas released is then calculated for each phase for each temperature heating step. The total ^{39}Ar and ^{40}Ar released in each laboratory heating step is the sum of the gas released from all the phases. The age spectra

is then determined from these summed values.

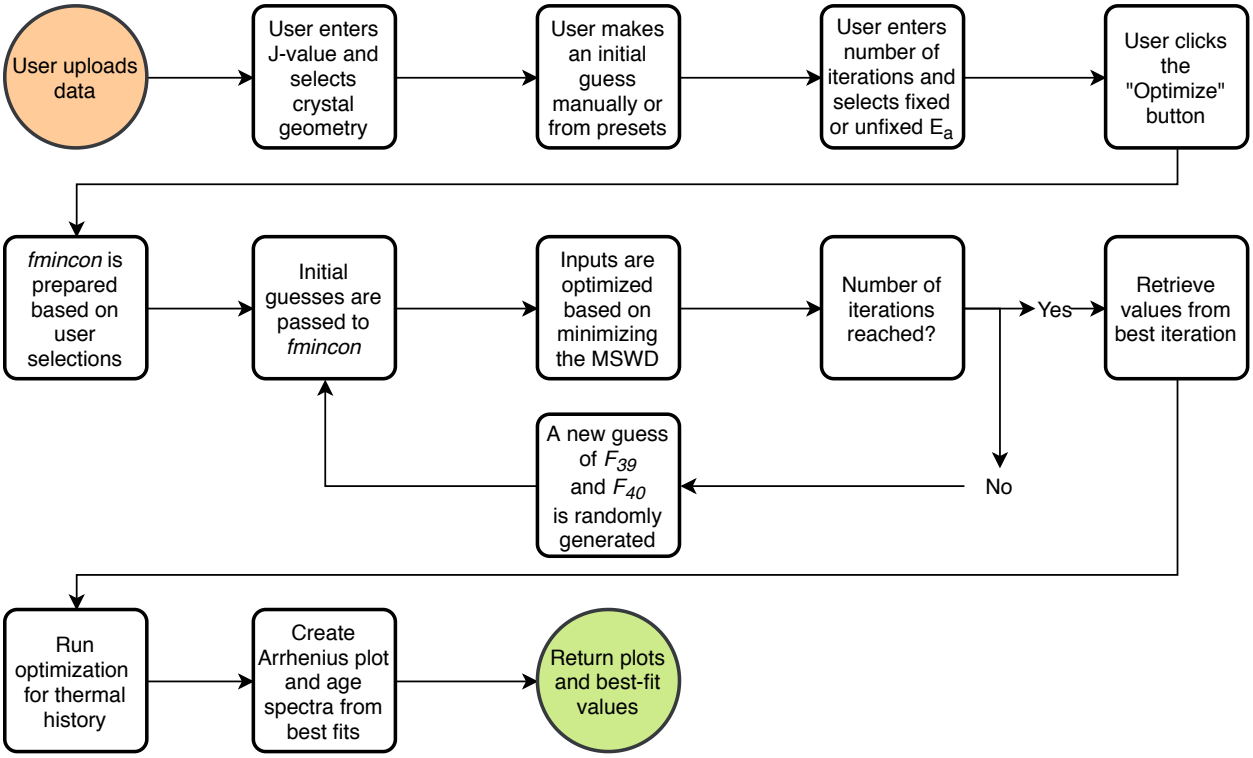

Figure 6: General programmatic flow of OPTIMuM. See text for details on specific steps and equations.

To determine the best fit values for E_a, $\ln(D_0/r^2)$, F_{39}, and F_{40}, I utilized a built-in optimization function in MATLAB, *fmincon*. This function incrementally changes the parameter values to minimize an associated error function. Here I use a mean square weighted deviation (MSWD) that incorporates the difference in $^{40}Ar/^{39}Ar$ ratio and f released in each step between the measured and modeled data. To avoid local minima, the software automatically creates a different initial guess by randomly generating a new F_{39} and F_{40} a user-defined number of times. I optimize these fractions separately as the ^{40}Ar will have a different distribution than the ^{39}Ar in samples with disturbed age spectra, which I am targeting in this study. The *fmincon* optimization routine is then run using each of these initial guesses. The best-fit values, i.e. those that return the lowest MSWD, are returned by the program.

Figure 7 shows a labeled image of the final GUI and table 2 shows the preset diffusion

values that the user can select. The presets are intended as a guideline that streamlines the initial guess process; the user may elect to optimize E_a since it has a range of values in nature. By default, the initial guess table populates with an evenly divided gas distribution across the phases. These values are not important for the initial guess since OPTIMuM will run its optimization routine for a user-defined number of iterations, where each run randomly picks a new starting point.

Figure 7: Labeled image of OPTIMuM's GUI with data (red) from Swindle et. al. (2009) sample LAP 031308A, thermal model (green), and ^{40}Ar distribution model (blue). See text for full model results.

3.2 *Thermal Modeling*

Optimization of the thermal parameters is currently coded in to the software, but needs further refinement before complete automation. Currently, the user can manually adjust the thermal parameters to fit the data and the optimized diffusion model. I will review this subject and future directions in the discussion.

Mineral	E_a (kJ/mol)	$\ln(D_0/r^2)$ (s^{-1})
Plagioclase	330	8
Pyroxene	1300	5
Manual entry	User-defined	User-defined

Table 2: Preset diffusion values in OPTIMuM for plagioclase and pyroxene. While these values have ranges in nature, these presets simplify the data entry process for the user. The user can select to fix these E_a values or to optimize them. Values adapted from Cassata, Renne, & Shuster (2009 & 2011).

The second step to the modeling is to use the diffusion kinetics constrained above to determine the thermal history that reproduces the currently observed gas quantities. I start by finding the minimum crystallization age (t_c) given the current F_{39} and F_{40} . This is done by rearranging the age equation to calculate the total amount of present-day $^{40}\mathrm{Ar_{ND}}$ assuming a t_c and no Ar loss (22). This value is then assumed to have the theoretical distribution between i phases of F_{39} (23).

$$^{40}Ar_{ND} = {}^{39}Ar\left(\frac{\exp(t_c * \lambda_{40K}) - 1}{J}\right) \tag{22}$$

$$^{40}Ar_{NDi} = {}^{39}Ar\left(\frac{\exp(t_c * \lambda_{40K}) - 1}{J}\right) F_{39i} \tag{23}$$

We can then determine the amount of gas loss by taking the difference between the theoretical no loss value of $^{40}\mathrm{Ar_{ND}}$ and the experimentally observed amount of $^{40}\mathrm{Ar_C}$ (24).

$$\Delta^{40}Ar = {}^{40}Ar_{ND} - {}^{40}Ar_C \tag{24}$$

If our assumption of t_c is too low, our $^{40}\mathrm{Ar_C}$ would be larger than the $^{40}\mathrm{Ar_{ND}}$, thus $\Delta^{40}Ar$ would be negative. The minimum t_c can be found such that $\Delta^{40}Ar$ is non-negative, an *a priori* and necessary constraint.

With a minimum t_c constrained, we can now optimize the parameters of a thermal event, such as an impact, that can reproduce the partial resetting we see in the samples. OPTIMuM currently uses a radiative cooling model such that cooling time is inversely proportional to temperature cubed. In this model, the three parameters being optimized are maximum

temperature (T_{max}), outgassing age (t_{out}), and α. For a given thermal history the amount of gas loss can now be calculated using equations from Turner (1968). For a given time and temperature, the Arrhenius relationship can be used to calculate the amount of diffusion x such that

$$x = \pi^2 \int_0^t \frac{D_0}{r^2} \exp\left(\frac{E_a}{T}\right) dt \tag{25}$$

which is then used to compute total fractional loss $f(x)$.

$$f(x) = 1 - \frac{6}{\pi^2} \sum_{n=1}^{\infty} \frac{1}{n^2} \exp\left(-n^2 x\right) \tag{26}$$

Appendix B shows graphically the relationship between cooling time, temperature, and (25)–(26). We now have all the quantities needed to model the currently observed $^{40}\mathrm{Ar_C}$, which comes from the amount of ^{40}Ar remaining after the thermal event plus the new ^{40}Ar formed since the event (figure 8). Equation (22) is used to find the $^{40}\mathrm{Ar_{ND}}$ assuming the minimum t_c. The age equation is then used again to compute the amount of ^{40}K originally present in the sample based on this total amount of ^{40}Ar. Next, the amount of ^{40}Ar at time of outgassing t_{out} is calculated using the following equation.

$$^{40}Ar_{out} = {}^{40}K(1 - \exp(-\lambda_{40K}(t_c - t_{out}))) \tag{27}$$

The amount of ^{40}Ar formed since the outgassing, $^{40}\mathrm{Ar_2}$, is then simply calculated by subtracting this value from the total amount of ^{40}Ar (28).

$$^{40}Ar_2 = {}^{40}Ar_{ND} - {}^{40}Ar_{out} \tag{28}$$

The modeled amount of ^{40}Ar present in each phase, can then be determined for a given thermal history using equation (29), where *f(x)* is calculated for each mineral phase using equations (25)–(26).

$$^{40}Ar_{pres} = (1 - f(x))({}^{40}Ar_{out}) + {}^{40}Ar_2 \tag{29}$$

For the optimization routine, I define the MSWD as the difference between the amount of ^{40}Ar in each phase determined using (29) and the previously determined F_{40}, from the

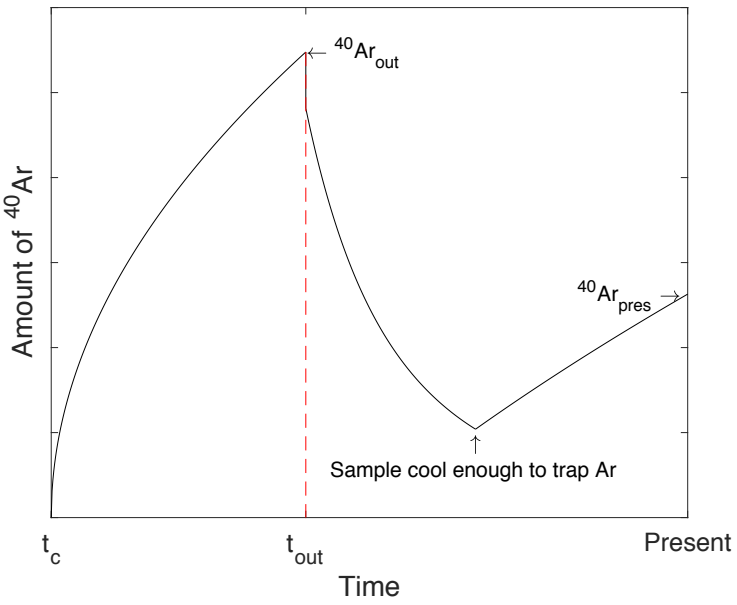

Figure 8: Hypothetical changes in amount of ^{40}Ar in a sample over time, assuming a thermal outgassing event at t_{out} (not to scale, exaggerated for detail). The sample gains ^{40}Ar from radioactive decay until it is heated at t_{out} by an impact, causing it to lose some amount of ^{40}Ar. The sample continues to lose ^{40}Ar until it sufficiently cools to begin trapping it again.

multi-phase kinetic modeling. For this optimization routine, I use the MATLAB function *patternsearch* to find the thermal history that results in the lowest MSWD. *Patternsearch* is similar to *fmincon*, however it uses an adaptive-mesh method instead of incremental changes in parameters. This function is better at handling scaling issues than *fmincon*, which is a bigger issue for the thermal modeling.

The final product of OPTIMuM is plots and tabulated values of the diffusion kinetics, the distribution of F_{39}, the distribution of F_{40}, and the most plausible thermal history for samples containing multiple-diffusion domains. In the following sections, I apply OPTIMuM to samples from three different planetary bodies to constrain their thermal histories as a first time in investigating impact environments throughout the inner solar system.

4 Results

I have used the optimization routine to find diffusion kinetics and manually fit thermal histories to model three samples in detail. Appendix C lists the data sets used for this

modeling. The number of phases is an assumption by the user; I place an upper limit on the number of phases by not allowing any phase to have ≤1% F_{39} and F_{40}. Below this fraction, a phase does not contribute significant amounts of gas and thus has negligible effects on the age spectrum and thermal modeling. I have also allowed OPTIMuM to optimize E_a to test it full capabilities. Future versions of the software may seek to constrain it more and users may elect to keep its value fixed during optimization. Table 3 summarizes the diffusion and thermal results.

4.1 *LAP 031308*

Swindle et al. (2009) originally collected $^{40}Ar/^{39}Ar$ analysis for H-chondrite LAP031308 from the LaPaz icefield, Antarctica. It is a clast-rich impact melt breccia, which makes it a good candidate sample for investigating impact heating in the asteroid belt. Using OPTIMuM, I have determined that this sample is best fit with four phases (figure 9) having ranges of E_a from 143.7–3053 kJ/mol and $\ln(D_0/r^2)$ from 0.999–100 s^{-1}. The two phases with lower E_a each contain about 1/3 of the ^{39}Ar, while the two phases with higher E_a combine to have over 1/2 of the ^{40}Ar. I interpret three phases as plagioclase with lower E_a and the other as pyroxene. While 3053 kJ/mol is on the upper end of pyroxene's natural range, this steep E_a phase helps to fit the high temperature part of the Arrhenius plot. This fit had an MSWD of 1.34. A five phases fit was attempted, but the additional phase contained a negligible amount of gas and thus is not considered. The best fit thermal model produced a t_c of 3.4 Ga, t_{out} of 1.237 Ga, T_{max} of 770°C, and α of 1E5.

4.2 *NWA 7034*

Cassata et. al. (2018) originally collected $^{40}Ar/^{39}Ar$ analysis for Martian meteorite NWA7034, a regolith breccia with some of the oldest samples of Martian crust (McCubbin et al., 2016). With OPTIMuM, I have produced four diffusion models for this sample: one with four phases, two with five phases, and one with six phases for completeness as well as to demonstrate the complexities in non-uniqueness for some samples (figure 9). All diffusion models indicate the presence of mostly plagioclase feldspar and some pyroxene, which is

Table 3: Summary of results

Sample	Source	Num. Phases	E_a	$\ln(D_0/r^2)$	F_{39}	F_{40}	t_c	t_{out}	T_{max}	α
LAP 031308	Swindle et. al. (2009)	4	1303	44.8	0.1853	0.3133	3.4	1.237	770	1E5
			143.7	0.999	0.3379	0.1057				
			616.6	20.6	0.3593	0.3650				
			3053	100	0.1175	0.2160				
NWA 7034	Cassata et. al. (2018)	4	343.3	12.4	0.3362	0.1939	4.5	1.45	1100	25587
			436.5	10.9	0.4503	0.2789				
			457.8	23.4	0.0936	0.0800				
			615.8	14.9	0.1199	0.4472				
NWA 7034	Cassata et. al. (2018)	5	331.7	12.0	0.3630	0.2101	4.5	1.45	1100	25587
			836.9	24.5	0.1013	0.5824				
			520.0	27.8	0.0639	0.0605				
			597.2	16.4	0.3928	0.0780				
			730.6	27.5	0.0790	0.0690				
NWA 7034	Cassata et. al. (2018)	5	300.8	6.88	0.2589	0.1327	4.5 4.5	1.45 1.25	1100 1440	25587 840
			843.9	41.2	0.1596	0.0871				
			418.1	20.5	0.1705	0.1268				
			450.8	9.06	0.1400	0.5204				
			573.6	15.9	0.2710	0.1329				
NWA 7034	Cassata et. al. (2018)	6	413.2	14.6	0.0353	0.1777	4.5	1.45	1100	25587
			403.0	19.0	0.1747	0.1480				
			651.5	18.7	0.2398	0.1612				
			354.8	11.9	0.2769	0.0066				
			316.5	5.39	0.2366	0.0945				
			729.2	19.6	0.0366	0.4121				
Apollo 16 69945	Norman et. al. (2006)	5	498.7	15.5	0.7161	0.7637	3.877	2.21	670	1900
			271.6	9.47	0.0654	0.0216				
			2099	70.0	0.0887	0.0762				
			1241	38.0	0.0680	0.0691				
			1274	68.4	0.0618	0.0694				

Table 3: Diffusion and thermal model results. Columns 1 and 2 describe sample information. Columns 3–7 are results of diffusion modeling showing number of phases, activation energy, frequency factor, and fractions of ^{40}Ar and ^{39}Ar in each phase. Columns 8–11 are thermal model results showing minimum crystallization age, outgassing age, maximum temperature, and parameter alpha. Diffusion parameters have same units as Table 2. Ages are in Ga and temperature is in °C.

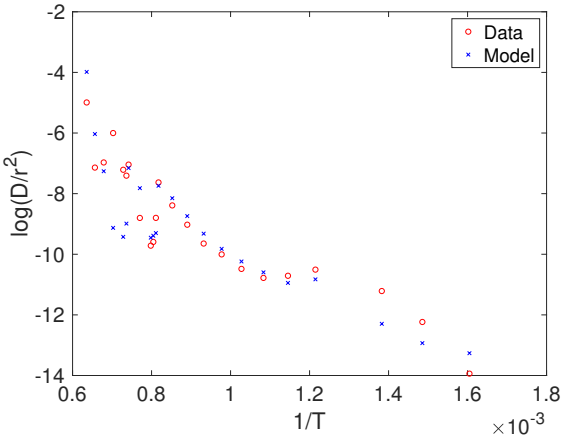

(a) LAP 031308 Arrhenius plot with 4 phases.

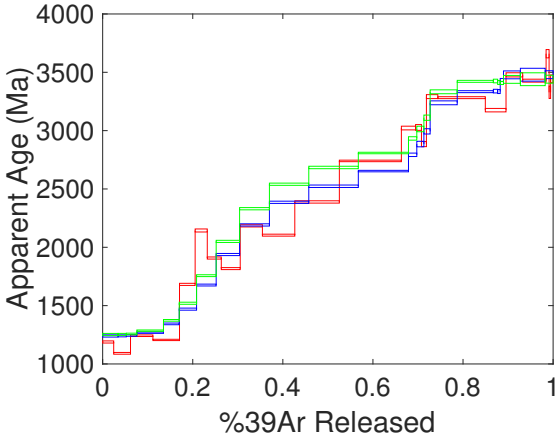

(b) LAP 031308 age spectrum with 4 phases.

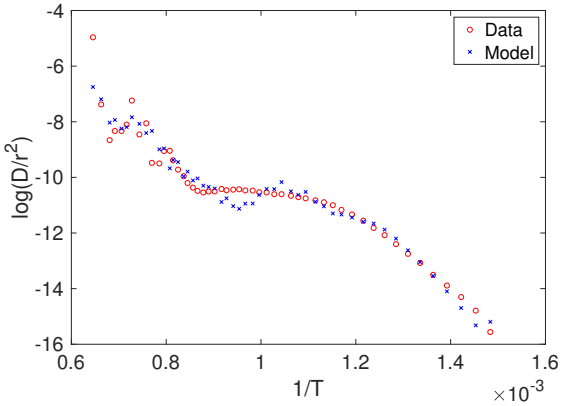

(c) NWA 7034 Arrhenius plot with 4 phases.

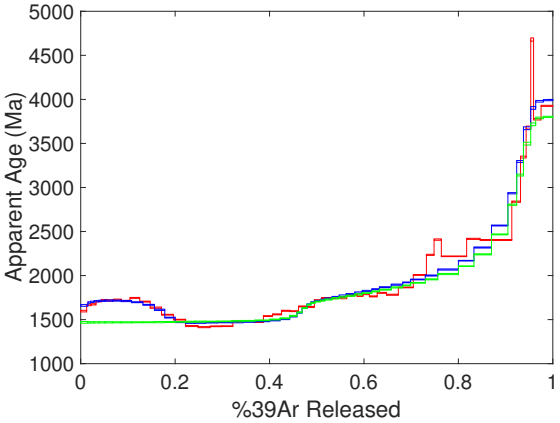

(d) NWA 7034 age spectrum with 4 phases.

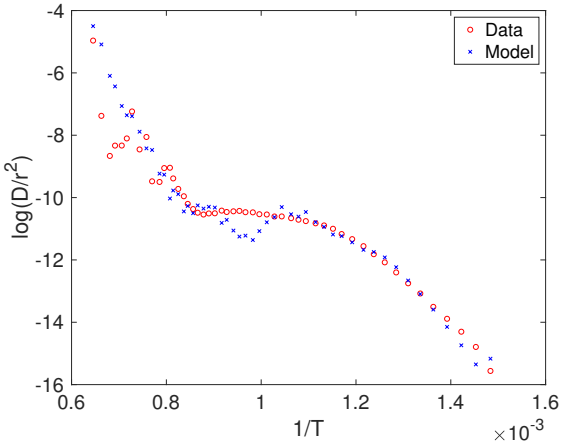

(e) NWA 7034 Arrhenius plot A with 5 phases.

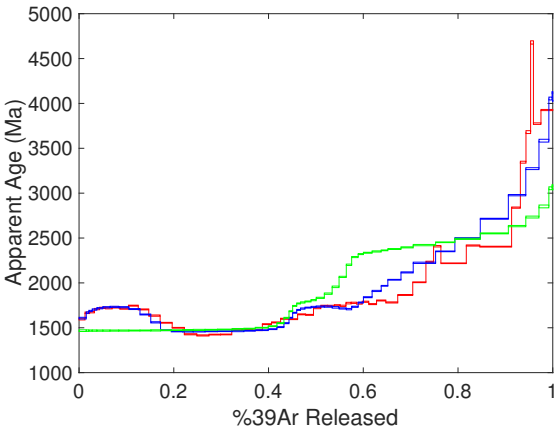

(f) NWA 7034 age spectrum A with 5 phases and same thermal parameters as (d).

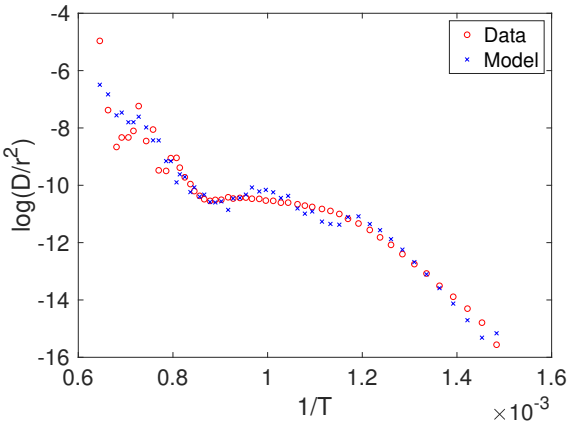

(g) NWA 7034 Arrhenius plot with 6 phases.

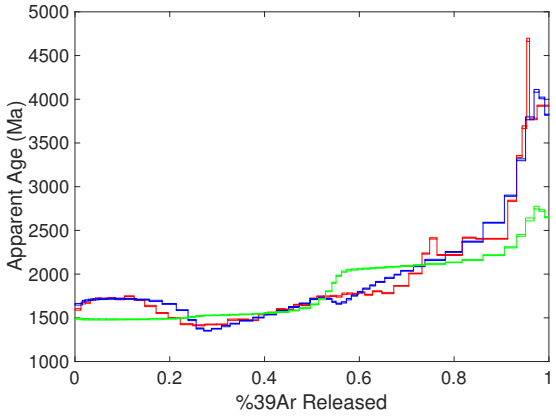

(h) NWA 7034 age spectrum with 6 phases and same thermal parameters as (d).

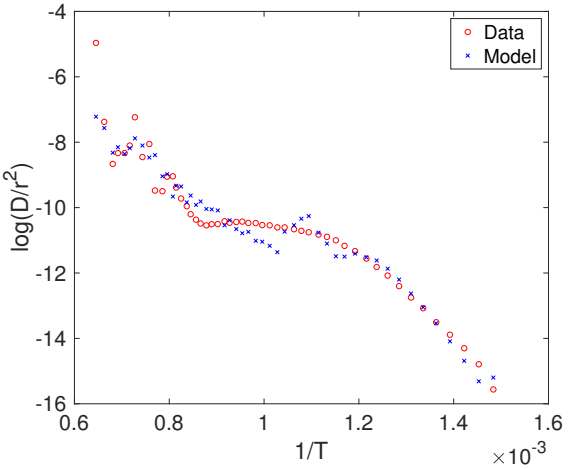

(i) NWA 7034 Arrhenius plot B with 5 phases.

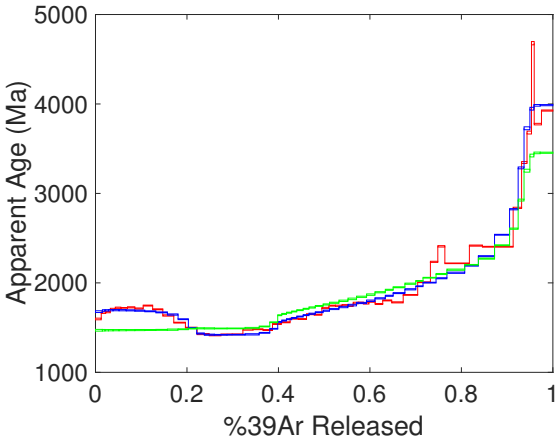

(j) NWA 7034 age spectrum B with 5 phases and same thermal parameters as (d).

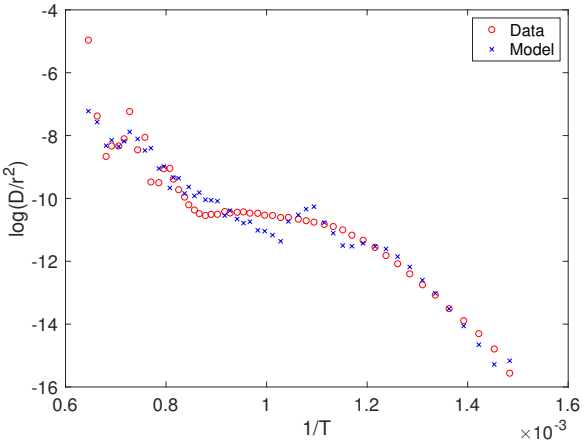

(k) NWA 7034 Arrhenius plot B with 5 phases.

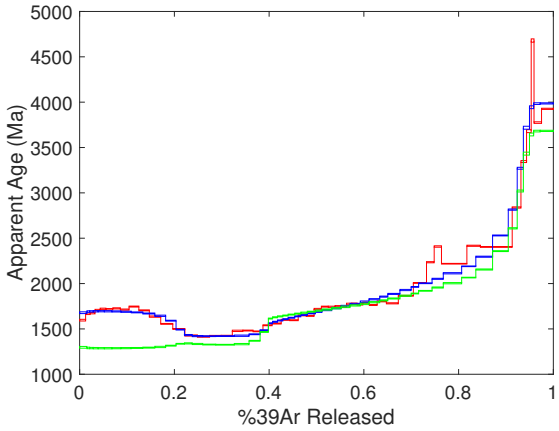

(l) NWA 7034 age spectrum B with 5 phases and different thermal parameters than (d).

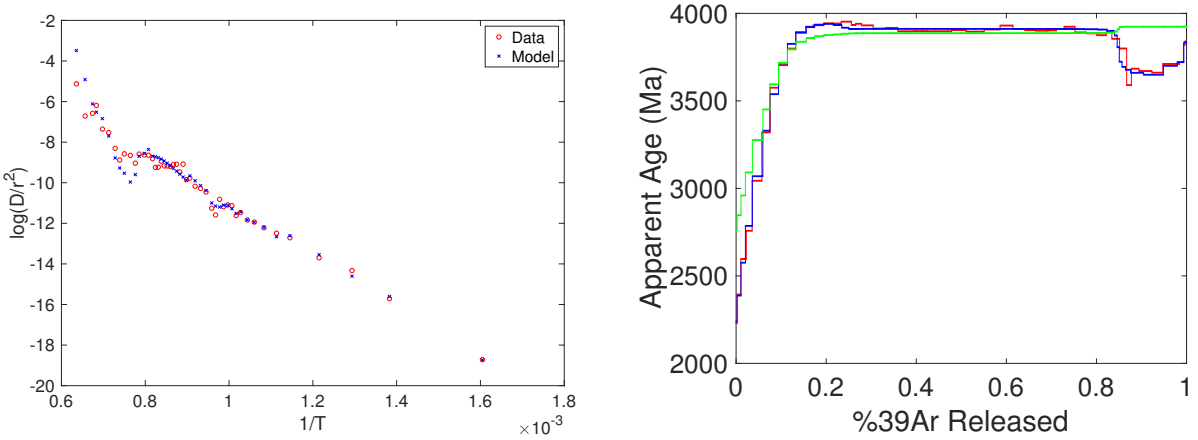

(m) Apollo 16 69945 Arrhenius plot with 5 phases. (n) Apollo 16 69945 age spectrum with 5 phases.

Figure 9: Arrhenius plots and age spectra with data (red), modeled ^{40}Ar distribution (blue), and thermal model (green).

consistent with the compositional interpretation in Cassata et al. (2018). The ranges of E_a and $\ln(D_0/r^2)$ for the four-phase fit, 343.3–615.8 kJ/mol and 10.9–23.4 s^{-1} respectively, are smaller than LAP 031308 and can be interpreted as all plagioclase. The two lower E_a phases contain a combined 75% of ^{39}Ar, while the two higher E_a phases contain a combined 52% of the ^{40}Ar, though the 457 kJ/mol phase contributes only 8% to this number. For the four-phase thermal model, I have fit a t_c of 4.5 Ga as well as an outgassing event with a t_{out} of 1.45 Ga, a T_{max} of 1100°C, and an α of 25587.

The five-phase fits, which I will call A and B for table 3 rows 3 and 4 respectively, have similar lower bounds on E_a to the four-phase fit, but the upper-most E_a is 843.9 kJ/mol, which could be a pyroxene phase. The values of E_a are higher on average compared to the four-phase fit, but the range of E_a between the two five-phase fits is nearly identical. Three of the phases in fit A (table 3, row 3) together contain over 80% of both Ar isotopes, while the other two each contain less than 8% of both Ar isotopes. Fit B (table 3, row 4) has more equal values of E_a, which indicates similar phase composition and crystallinity. The MSWDs of the five-phase diffusion models are 1.85 (A) and 0.44 (B), compared to 0.44 for the four-phase; the uncertainties and errors will be explored in the discussion.

The best fit for the thermal history is similar to that of the four phase model, however

the data is, qualitatively, fit best with the five-phase B model. For five-phase model B, I have also included a second thermal model (figure 9l), which I will call thermal model B, with a t_{out} of 1.25 Ga, T_{max} of 1440°C, and α of 840. It is clear that the thermal model is affected more by the diffusion kinetics than the number of phases, and that different thermal parameters will fit different parts of the age spectra.

Five-phase model B (figures 9i, j) is more appealing because thermal model A has a much better fit compared to the five-phase model A with the same thermal model. This model is the most compelling of the models because of its low MSWD and reasonable distribution of gas. It fits most of the age spectrum well, especially in the last 50%. Its fit in the first 5% is slightly worse than the first two models, but this difference is minor. The six-phase model fits the final spike as well as the middle third of the age spectrum. However, the thermal model has a poor fit and the distribution of gas in the fourth phase would suggest a second, recent heating event, which is beyond OPTIMuM's current capabilities. I therefore favor the second five-phase fit as the most likely.

4.3 *Apollo 16 69945*

The last sample included in this study is Apollo 16 impact melt rock 69945 originally studied by Norman, Duncan, and Huard (2006). The best fit for this sample uses five phases ranging in E_a from 271–2099 kJ/mol and $\ln(D_0/r^2)$ from 9.47–70.0 s^{-1}. The phase with E_a of 498.7 kJ/mol dominates the gas release for both ^{40}Ar and ^{39}Ar, with 76.3% and 71.6% gas respectively. All the remaining phases have <9% of each isotope. The two lower E_a phases can be interpreted as plagioclase, while the three higher E_a phases can be interpreted as pyroxene, which is generally consistent with the mafic composition identified in Norman et al. (2006). The two 1200 kJ/mol phases are nearly identical except for the higher frequency factor in the 1274 kJ/mol phase, which helps fit the upper part of the Arrhenius plot. The MSWD for this model is exceptionally low at 0.04 and there seems to be a less obvious tradeoff between the Arrhenius plot and age spectra. The age spectra is fit well all the way through, including the dip at 80%, while the Arrhenius plot has a close fit except for a small

region around $1/T$ of 0.75.

A t_c of 3.887 Ga, and a thermal event with t_{out} 2.21 Ga, T_{max} of 670°C, and α of 1900 fit the first 80% of gas release. After this point however, the fit becomes poor, which indicates that other factors may have affected this sample; this will be discussed further in the next section.

5 Discussion

The type of thermal modeling I have conducted is difficult and has only been attempted by a few others recently (e.g. Boehnke et al., 2016; Cassata et al., 2018; Weirich et al., 2012). My models provide valuable information about the collision history of extraterrestrial bodies and are an important first step in developing software that will allow for this modeling to be applied to a large suite of extraterrestrial and terrestrial samples. In this section I will discuss the implications of the thermal models for each sample, the uncertainties for the model fits, and next steps that will expand the application of OPTIMuM.

5.1 *LAP 031308*

Although LAP 031308 does not appear to contain a 'plateau' age, I determined a minimum crystallization of 3.4 Ga. This value is slightly below the minimum impact age for the H-chondrite parent body of 3.6 Ga inferred by Wittmann et al. (2010), which suggests this sample may have experienced total degassing during this impact event. Swindle et al. (2009) report an outgassing event age of 752±47 Mya based on the age spectra alone, however there is no further discussion of this sample due to its disturbed nature. The authors instead focus on two other samples from LAP 031308 that show less Ar-loss. Therefore, OPTIMuM has placed new constraints on this sample by revealing a possible event 500 My before the one in Swindle et al. (2009). The maximum temperature from the thermal model of 770°C matches well with the (non-shock) peak temperatures of about 770°C derived based on the petrology of this sample by Wittmann et al. (2010). My results therefore suggest that this sample was completely degassed at least 3.4 Ga and was then subsequently heated at ∼1.24 Ga to

770°C during an impact event.

5.2 *NWA 7034*

Five-phase fit B with thermal model A for NWA 7034 generally agrees with Cassata et. al. (2018). The minimum crystallization age of 4.5 Ga suggest formation on early Mars and is consistent with ages from other techniques, such as Sm-Nd, U-Xe, and U-Pb (Cassata et al., 2018; Humayun et al., 2013). Likewise, the outgassing age of 1.45 Ga agrees with the Amazonian heating that Cassata et al. (2018) report, although it is on the upper end of their range, which goes up to 1.5 Ga. They also speculate that low-temperature volcanic metamorphism may have caused this event. My model's T_{max} of 1100°C indicates that it may have briefly experienced high temperatures, but cooled rapidly to more moderate temperatures as indicated by a relatively large α.

It is important to note the differences in the thermal models for NWA 7034. The diffusion parameters have a clear affect on the same thermal models as seen in figure 8. I am still working to further constrain the relationship between the diffusion kinetics and thermal history. Future releases of OPTIMuM will ideally optimize diffusion and thermal parameters jointly and provide a range of solutions to handle non-uniqueness.

5.3 *Apollo 16 69945*

For Apollo 16 breccia 69945, the thermal model is less clear cut than the other two samples. In previous samples, the age has increased with increasing fraction of ^{39}Ar loss. Sample 69945 is different in that there is a decrease in age during the last 20% of the age spectra. Despite adjusting all parameters of the thermal model, this dip from the plateau was unable to be fit with the radiative cooling model. Similar high temperature Ar-loss is observed in many meteorite, Martian, and lunar samples, and Cassata et. al. (2010) and Boehnke et al. (2016) suggest that this is a result of impact heating. For example, Cassata et al. (2010) reproduced the high temperature Ar-loss in Martian sample ALH 84001 using a thermal pulse with a peak temperature of >1400°C for ≤1 second, which can only be produced in a shock environment. OPTIMuM does not currently have the option to use this

type of thermal history; I, therefore, focused on fitting the first 80% of the age spectra, which resembles a slowly cooled sample. I determined a minimum crystallization age of 3.877 Ga that is consistent with the crystallization age determined by Norman et al. (2006). This sample is an impact melt breccia, so these results suggest it crystallized as a result of an impact around 3.877 Ga. The thermal modeling also suggests that this samples subsequently heated at ∼2.21 Ga with a peak temperature of 670°C.

5.4 *Uncertainties*

For the diffusion kinetics modeling, the MSWD quantifies the error in the fit and measures its overall quality. The apparent ages of each step contain errors shown by the vertical width of the boxes in the age spectra (e.g. figure 8). The uncertainties in laboratory temperatures, decay constants, etc. will be the same for each step in the age spectrum. The main contribution to the uncertainties in each step is therefore the counts of Ar released in each step and the associated counting statistical uncertainties. OPTIMuM currently uses a χ^2 test to constrain the goodness of fit, so the uncertainties are not propagated into the model. One of the next steps for OPTIMuM is to use a reduced χ^2 fit, which would weight each step by the uncertainties. However, for the three samples I analyzed, the uncertainties do not vary significantly between each step, so this change would not change the results of the thermal model discussed in the previous section.

Boehnke et al. (2016), published MDD modeling similar to mine, discuss a tradeoff in trying to fit both an Arrhenius plot and an age spectra. As with any inverse modeling problem, there is a possibility that there are multiple solutions that could be considered a best fit. Boehnke et al. (2016) tried to simultaneously fit both the diffusion kinetics and the thermal histories and found that one dimension (e.g. the age spectra) can have a significantly better fit than the other dimension (e.g. the Arrhenius plot) while producing a small MSWD. Unlike previous work, OPTIMuM uses a three step approach where the diffusion kinetics are fit first using the ^{39}Ar data. The diffusion kinetics and the age spectrum are then used to determine the current distribution of ^{40}Ar in the sample. Finally, the program models

the thermal history necessary to produce the observed, current ^{40}Ar distribution assuming a crystallization age. Using this three step approach, I have was generally able to overcome the trade off in optimization reported by Boehnke et al. (2016).

In order to fully interpret the thermal model results and to use them to address questions of impact bombardment, the uncertainties on the modeled parameters need to be estimated. In addition, there may be correlations between the parameters. For example, lowering alpha and raising t_c may produce multiple best fit age spectra. I have started investigating the uncertainties in the model parameters, however, this part of the project is ongoing. Below, I describe the approach I am taking and the initial results.

Figure 10 shows the method I am using to estimate the model uncertainties. For each plot I vary only one modeled parameter for only one phase, while keeping all other parameters fixed and calculate the MSWD. This type of plot reveals the best fit value with the lowest MSWD (bottom red line in figure 10) and a simple estimate of errors as the input values that correspond to the minimum MSWD plus one (top red line in figure 10). In the two examples in Figure 10, the activation energies are constrained to 1303 +300/-100 *kJ/mol* and 143.7 +20/-10 *kJ/mol*. Phase one is clearly in the range of pyroxene activation energies and phase two is consistent with the range of plagioclase values. This suggests that my modeling is producing unique fits to the diffusion kinetics that are consistent with the known mineralogy of the sample. My ongoing work includes conducting this type of error analysis and investigating correlations between all the fit parameters. Eventually, OPTIMuM's GUI will include a separate tab with uncertainties.

6 Summary & Future Work

Using the MDD method of ^{40}Ar/^{39}Ar modeling, I have created new software that models the diffusion kinetics and thermal histories of bulk samples. This software is especially advantageous for extraterrestrial samples, which are often too fine grained to do mineral separates. With this software, I have modeled a chondritic meteorite, a Martian meteorite, and a lunar impact melt rock. With E_a allowed to optimize, the models show a spread of

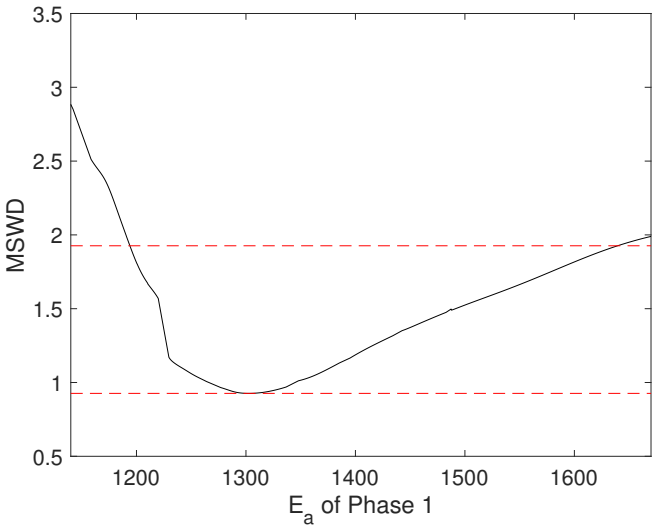

(a) MSWD plot for LAP031308 phase one.

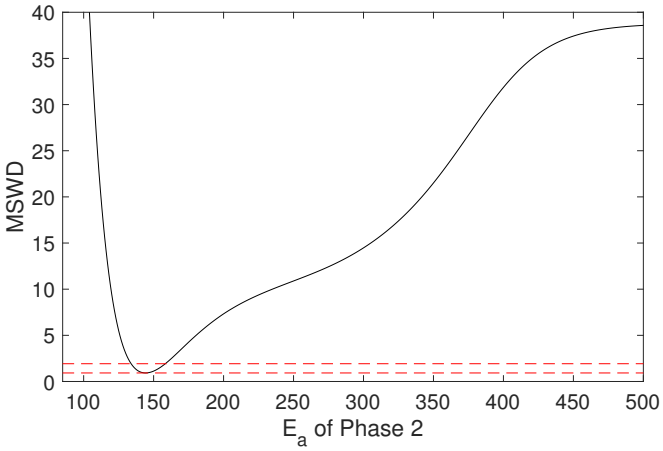

(b) MSWD plot for LAP031308 phase two.

Figure 10: MSWD plots for phases one (top) and two (bottom) of LAP031308. Lower dashed line is the minimum MSWD value and upper dashed line is minimum MSWD plus one.

values generally consistent with plagioclase or pyroxene, though there are some outliers (e.g. LAP 031308 phase four). Importantly, the diffusion models have helped constrain radiative-based thermal models for the three samples. Both LAP031308 and NWA 7034 have similar outgassing ages, but NWA 7034 both crystallized ∼1 Ga before LAP 031308 and outgassed at a higher temperature. The thermal model for Apollo 69945 fits the first 80% of the age spectra well, but the digression in the final 20% of the age spectrum shows the need for either a second thermal event or different cooling model (i.e. impact shock heating). Still, the Apollo 69945 results are consistent with a low temperature heating event around 2.21 Ga.

Future work will continue to build on OPTIMuM's current foundation. The optimization options can be expanded to allow the user to modify the constraints on *fmincon*. It will also be necessary define an optimization routine for the thermal models. *Patternsearch* has shown potential so far, but a more appropriately scaled objective function will ultimately lead to the most accurate results. Once this is in place, additional types of thermal models, such as shock heating, could be integrated in to the software as well. Estimates of error will also be more robust in future versions of OPTIMuM by using MSWD plots like the ones shown in figure 10. This will constrain a range of diffusion parameters and reduce non-uniqueness in the thermal models.

One final note is that many data sets were either missing critical data or were not reported at all. Data and experimental procedures should be fully published to allow for new analyses and modeling through software like OPTIMuM. I recommend that at a minimum for $^{40}Ar/^{39}Ar$ studies, the temperature, step-heating time, J-value, and amounts of each isotope be published both uncorrected and corrected for cosmogenic components.

References

Bell, E. A., Harrison, T. M., Kohl, I. E., and Young, E. D. (2014). "Eoarchean crustal evolution of the Jack Hills zircon source and loss of Hadean crust". In: *Geochimica et Cosmochimica Acta* 146, pp. 27–42.

Boehnke, P., Harrison, T. M., Heizler, M. T., and Warren, P. H. (2016). "A model for meteoritic and lunar 40Ar/39Ar age spectra: Addressing the conundrum of multi-activation energies". In: *Earth and Planetary Science Letters* 453, pp. 267–275.

Boehnke, P. and Harrison, T. M. (2016). "Illusory Late Heavy Bombardments". In: *Proceedings of the National Academy of Sciences* 113.39, pp. 10802–10806.

Cassata, W. S., Cohen, B. E., Mark, D. F., Trappitsch, R., Crow, C. A., Wimpenny, J., Lee, M. R., and Smith, C. L. (2018). "Chronology of martian breccia NWA 7034 and the formation of the martian crustal dichotomy". In: *Science Advances* 4.5, eaap8306.

Cassata, W. S., Renne, P. R., and Shuster, D. L. (2009). "Argon diffusion in plagioclase and implications for thermochronometry: A case study from the Bushveld Complex, South Africa". In: *Geochimica et Cosmochimica Acta* 73.21, pp. 6600–6612.

— (2011). "Argon diffusion in pyroxenes: Implications for thermochronometry and mantle degassing". In: *Earth and Planetary Science Letters* 304.3, pp. 407–416.

Cassata, W. S., Shuster, D. L., Renne, P. R., and Weiss, B. P. (2010). "Evidence for shock heating and constraints on Martian surface temperatures revealed by 40Ar/39Ar thermochronometry of Martian meteorites". In: *Geochimica et Cosmochimica Acta* 74.23, pp. 6900–6920.

Cohen, B. A., Swindle, T. D., and Kring, D. A. (2005). "Geochemistry and 40Ar-39Ar geochronology of impact-melt clasts in feldspathic lunar meteorites: Implications for lunar bombardment history". In: *Meteoritics & Planetary Science* 40.5, pp. 755–777.

Harrison, T. M. and Lovera, O. M. (2014). "The multi-diffusion domain model: past, present and future". In: *Geological Society, London, Special Publications* 378.1, pp. 91–106.

Harrison, T. M. and Zeitler, P. K. (2005). "Fundamentals of noble gas thermochronometry". In: *Reviews in Mineralogy and Geochemistry* 58.1, pp. 123–149.

Humayun, M., Nemchin, A., Zanda, B., Hewins, R. H., Grange, M., Kennedy, A., Lorand, J.-P., Göpel, C., Fieni, C., and Pont, S. (2013). "Origin and age of the earliest Martian crust from meteorite NWA 7533". In: *Nature* 503.7477, p. 513.

Kelley, S. (2002). "K-Ar and Ar-Ar Dating". In: *Reviews in Mineralogy and Geochemistry* 47.1, pp. 785–818.

Kunz, J., Falter, M., and Jessberger, E. K. (1997). "Shocked meteorites: Argon-40-argon-39 evidence for multiple impacts". In: *Meteoritics & Planetary Science* 32.5, pp. 647–670.

Lovera, O. M. (1992). "Computer programs to model 40Ar/39Ar diffusion data from multidomain samples". In: *Computers & Geosciences* 18.7, pp. 789–813.

Lovera, O. M., Richter, F. M., and Harrison, T. M. (1989). "The 40Ar/39Ar thermochronometry for slowly cooled samples having a distribution of diffusion domain sizes". In: *Journal of Geophysical Research: Solid Earth* 94 (B12), pp. 17917–17935.

McCubbin, F. M., Boyce, J. W., Novák-Szabó, T., Santos, A. R., Tartèse, R., Muttik, N., Domokos, G., Vazquez, J., Keller, L. P., and Moser, D. E. (2016). "Geologic history of Martian regolith breccia Northwest Africa 7034: Evidence for hydrothermal activity and lithologic diversity in the Martian crust". In: *Journal of Geophysical Research: Planets* 121.10, pp. 2120–2149.

McDougall, I. and Harrison, T. M. (1999). *Geochronology and Thermochronology by the 40Ar/39Ar Method*. Oxford University Press on Demand.

Merrihue, C. and Turner, G. (1966). "Potassium-argon dating by activation with fast neutrons". In: *Journal of Geophysical Research (1896-1977)* 71.11, pp. 2852–2857.

Norman, M. D., Duncan, R. A., and Huard, J. J. (2006). "Identifying impact events within the lunar cataclysm from 40Ar–39Ar ages and compositions of Apollo 16 impact melt rocks". In: *Geochimica et Cosmochimica Acta* 70.24, pp. 6032–6049.

Reimink, J. R., Davies, J. H. F. L., Chacko, T., Stern, R. A., Heaman, L. M., Sarkar, C., Schaltegger, U., Creaser, R. A., and Pearson, D. G. (2016). "No evidence for Hadean continental crust within Earth's oldest evolved rock unit". In: *Nature Geoscience* 9.10, pp. 777–780.

Shuster, D. L., Balco, G., Cassata, W. S., Fernandes, V. A., Garrick-Bethell, I., and Weiss, B. P. (2010). "A record of impacts preserved in the lunar regolith". In: *Earth and Planetary Science Letters* 290.1, pp. 155–165.

Steiger, R. H. and Jäger, E. (1977). "Subcommission on geochronology: Convention on the use of decay constants in geo- and cosmochronology". In: *Earth and Planetary Science Letters* 36.3, pp. 359–362.

Swindle, T. D., Isachsen, C. E., Weirich, J. R., and Kring, D. A. (2009). "40Ar-39Ar ages of H-chondrite impact melt breccias". In: *Meteoritics & Planetary Science* 44.5, pp. 747–762.

Swindle, T. D., Kring, D. A., and Weirich, J. R. (2014). "40Ar/39Ar ages of impacts involving ordinary chondrite meteorites". In: *Geological Society, London, Special Publications* 378.1, pp. 333–347.

Turner, G. (1968). "The Distribution of Potassium and Argon in Chondrites". In: *Origin and Distribution of the Elements*. Ed. by L. H. Ahrens. International Series of Monographs in Earth Sciences. Pergamon, pp. 387–398.

Wittmann, A., Swindle, T. D., Cheek, L. C., Frank, E. A., and Kring, D. A. (2010). "Impact cratering on the H chondrite parent asteroid". In: *Journal of Geophysical Research: Planets* 115 (E7).

Appendix A: Data Template

	A	B	C	D	E	F	G	H	I	J	K	L	M	N
1	Temperature (˚C)	Step Duration (s)	Ar-40	Ar-40_Er	Ar-39	Ar-39_Er	Ar-38	Ar-38_Er	Ar-37	Ar-37_Er	Ar-36	Ar-36_Er	Ar40/Ar39	Ar40/Ar39_Er
2	400.856	80	25394.4262	38.6960371	251.732694	4.29030566	9.06723173	0.99352488	-0.0563881	26.2736189	36.3066348	2.25733752	100.878539	1.726141309
3	415.137	80	20945.588	42.7017938	194.555817	2.88700746	2.8957085	1.01456522	-0.0435805	26.3254551	22.1737991	2.23993113	107.658503	1.612547786
4	429.985	80	21762.2033	37.3936946	200.915696	2.5770183	3.88818473	1.15630188	-0.0450051	26.3254145	18.5529664	1.92954003	108.315098	1.401700232
5	445.17	80	24368.7009	56.9678736	217.975738	2.81012701	5.75017026	1.03498664	-0.0488266	26.0783147	18.1425153	2.22059864	111.795474	1.464763098
6	460.463	80	27477.6128	61.8210241	242.777502	2.8933844	3.57908241	1.11781003	-0.0543822	27.6524188	20.1640581	2.9305911	113.180227	1.372689599
7	475.53	80	32715.5182	65.7674755	290.203519	3.57527316	7.09557945	0.97047203	-0.0650056	27.3596863	29.5753088	2.98642036	112.733017	1.407225698
8	490.193	80	36310.0468	62.9634569	319.504069	3.49244247	8.40152516	1.00042335	-0.0715689	26.2736384	21.944387	2.11943526	113.645021	1.257767654
9	505.188	80	41059.723	67.4148785	365.694551	4.03178607	7.78474461	1.15519607	-0.0819156	26.3525916	26.3539256	2.29656146	112.278739	1.251525701
10	520.063	80	47680.3491	67.0513408	412.223396	3.77175282	9.68763501	1.09750189	-0.092338	26.1575155	33.869381	1.96558309	115.666286	1.070747731
11	534.907	80	49316.1968	75.711091	442.674414	4.13544407	7.32150941	1.05922427	-0.0991591	26.1575427	41.6389989	2.31764093	111.405121	1.054701182
12	549.35	80	50184.2798	72.8876635	479.703352	6.10961912	8.85244991	1.14338611	-0.1074536	26.4992937	30.9217667	2.29965188	104.615237	1.341040795
13	565.785	80	49313.2391	52.7320208	508.130347	4.32979623	8.0985672	1.18666985	-0.1138212	28.1361305	23.4454054	1.72778113	97.0484037	0.833438964
14	581.735	80	47107.926	66.1475469	512.327609	4.05959127	8.33254722	1.17779308	-0.1147614	26.4392414	15.7752058	2.06299521	91.9488335	0.739937363
15	595.304	80	45029.556	66.1348779	526.093237	6.40450249	6.1778945	1.11598615	-0.1178449	26.5000563	16.5854199	2.1865211	85.592349	1.049531511
16	609.711	80	43333.0856	85.3791432	512.885592	6.30639561	6.30149691	1.14865849	-0.1148864	26.7008186	8.81448656	1.93925948	84.4887949	1.052119619
17	623.878	80	41609.4839	62.5133462	487.789821	4.14431648	6.79342767	1.28074544	-0.1092649	26.4700469	11.832177	2.10351495	85.3020751	0.735979732
18	640.77	80	40203.3164	72.172943	470.691387	3.78371364	9.46970614	1.26979301	-0.1054349	26.5660644	10.7498298	2.89956808	85.413325	0.703519137
19	653.896	80	40208.4541	49.0072374	446.415033	6.39393622	9.33197445	1.19685516	-0.099997	26.4721505	13.6821231	2.99358172	90.0696687	1.294717009
20	667.462	80	38718.2172	58.4213934	428.445322	3.8636025	9.55140483	1.17968031	-0.0959718	26.5674318	10.5637812	2.29472513	90.3690979	0.826252918
21	685.304	80	37349.4456	46.6606058	417.028588	3.42439666	10.3263519	1.13812893	-0.0934144	26.6694999	16.4157156	2.05723106	89.5608757	0.743884654
22	699.608	80	36848.4087	61.3958403	385.338596	3.50406207	8.82804785	1.25523383	-0.0863158	26.9713414	14.438749	1.85763892	95.6260523	0.884048215
23	715.167	80	37227.911	68.959639	382.148543	3.85511254	11.7834718	1.11346168	-0.0856013	26.7780263	16.8203738	1.95181947	97.4173833	0.999176115
24	730.678	80	36439.7272	63.7267887	359.979305	3.76242518	9.17047553	0.98030754	-0.0806354	26.535073	10.3544666	3.33220549	101.227284	1.0727138
25	744.774	80	36075.2588	61.8067088	357.819931	3.15886616	9.6768981	1.09182258	-0.0801517	26.8901241	13.9530699	2.11908707	100.81959	0.906650413
26	761.137	80	35789.8835	38.3363827	337.684686	3.15498315	10.2281414	1.13841587	-0.0756414	26.5015446	10.2936614	2.60286058	105.986102	0.996713183
27	774.982	80	34935.758	64.1354773	331.444423	3.15382487	4.54531916	1.04307903	-0.0742436	26.8494653	11.5036795	2.6892602	105.404574	1.021462025

Figure A1: Minimum data required to run OPTIMuM. Units for amounts of gas need only be consistent between each other. Columns with 'Er' are for errors associated with the value, and changing column names will not affect the software. Addition of extra data columns will not affect the software as long as all columns are the same length. The current version of the software uses only temperature, time, ^{40}Ar, ^{39}Ar, and ^{40}Ar/^{39}Ar , but the other isotopes can be used in future iterations to include isochron plots, Ca/K plots, etc. If any non-essential isotope values are unknown, then non-negative placeholder values should be populated instead.

Appendix B: Cooling Curve

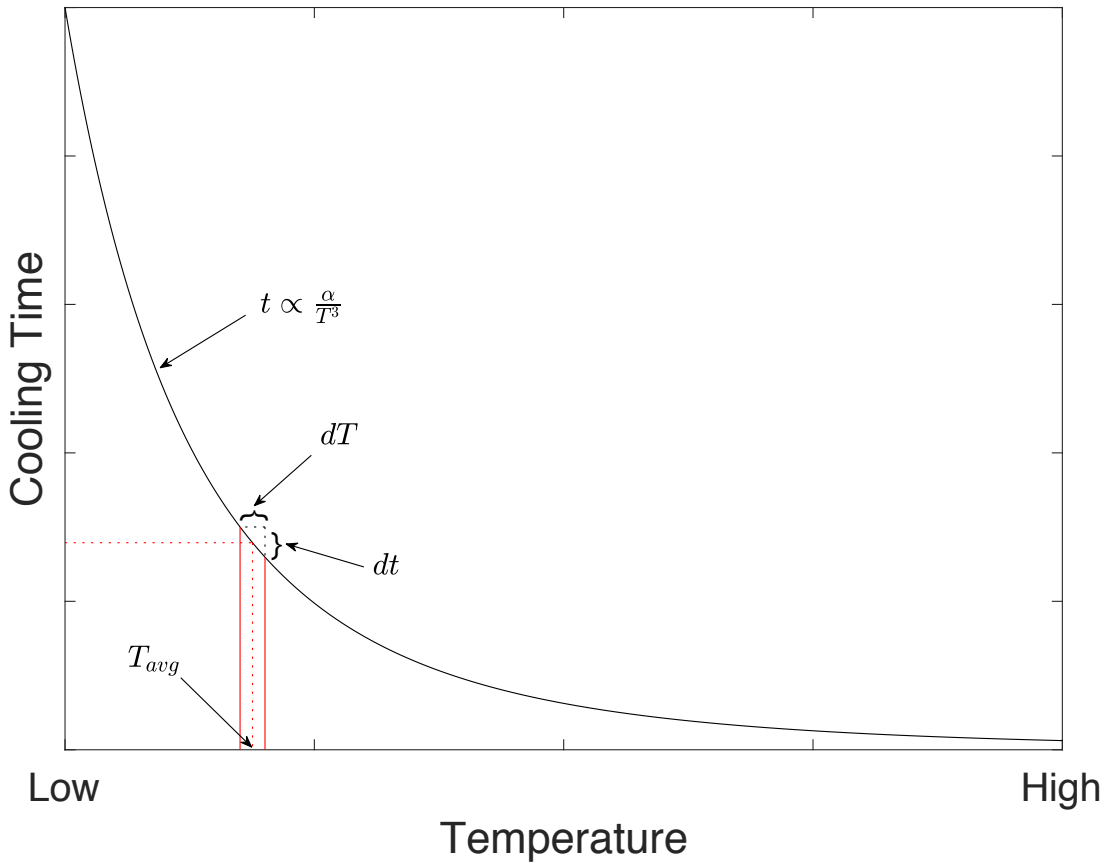

Figure B1: Plot showing cooling time as a function of temperature assuming radiative cooling (generated from artificial data). The cooling time is proportional to rate α and $1/T^3$. OPTIMuM calculates cooling histories by defining a temperature step (dT) and finding the cooling time for each step (dt). The Arrhenius relationship, the average temperature within each step (T_{avg}), and dt are then used to determine D/r^2. Equations (25) and (26) are then be used to calculate the fractional loss of Ar as the sample cools. This approach was taken so that it will be easier to expand OPTIMuM to include more complicated thermal histories (i.e. shock and radiative cooling).

Appendix C: Datasets

$$J = 0.002144 \pm 0.000004$$

Temperature (˚C)	Step Duration (s)	Ar-40	Ar-40_Er	Ar-39	Ar-39_Er	Ar40/Ar39	Ar40/Ar39_Er
350	60	1055.4	21.9	2.48	0.051	426.4	8.9
400	60	1433.6	26.2	3.77	0.069	380.1	6.9
450	60	2275.7	33.7	5.03	0.074	452.8	6.7
550	60	2595.3	32.3	5.97	0.074	434.9	5.4
600	60	2463.8	40.1	3.51	0.057	702.8	11.4
650	60	2827.6	57.9	2.72	0.056	1038.4	21.3
700	60	2691.1	40.7	3.14	0.047	856.3	12.9
750	60	3367.3	49.7	4.25	0.063	792.3	11.7
800	60	5332.5	79.4	4.98	0.074	1071.4	15.9
850	60	7307.9	97.3	7.27	0.097	1005.8	13.4
900	60	12530.8	185.1	10.00	0.148	1253.5	18.5
950	60	22511.3	202.3	13.91	0.125	1617.9	14.5
960	60	6261.9	133.9	3.19	0.068	1964.8	42.0
970	60	2601.7	87.2	1.32	0.044	1971.2	66.0
980	60	1985.7	59.4	1.11	0.033	1788.6	53.5
1025	60	6026.2	133.3	2.56	0.057	2350.2	52.0
1075	60	24884.9	265.1	10.65	0.113	2336.2	24.9
1085	60	10106.6	197.6	4.64	0.091	2177.0	42.6
1100	60	9917.0	225.4	3.74	0.085	2652.4	60.3
1150	60	13488.6	218.6	5.25	0.085	2568.6	41.6
1200	60	1999.8	89.7	0.67	0.030	2976.7	133.6
1250	60	815.1	56.0	0.34	0.023	2407.7	165.3
1300	60	1466.5	63.3	0.57	0.024	2594.8	112.1

Figure C1: Laboratory data for LAP 031308A from Swindle et al. (2009). Units for ^{40}Ar and ^{39}Ar are in $10^{-10}cc/g$. The values reported here are the only ones used for analyses in this paper.

$$J = 0.0138 \pm (3.68 * 10^{-5})$$

Temperature (˚C)	Step Duration (s)	Ar-40	Ar-40_Er	Ar-39	Ar-39_Er	Ar40/Ar39	Ar40/Ar39_Er
400.856	80	25394.43	38.70	251.73	4.29	100.88	1.73
415.137	80	20945.59	42.70	194.56	2.89	107.66	1.61
429.985	80	21762.20	37.39	200.92	2.58	108.32	1.40
445.17	80	24368.70	56.97	217.98	2.81	111.80	1.46
460.463	80	27477.61	61.82	242.78	2.89	113.18	1.37
475.53	80	32715.52	65.77	290.20	3.58	112.73	1.41
490.193	80	36310.05	62.96	319.50	3.49	113.65	1.26
505.188	80	41059.72	67.41	365.69	4.03	112.28	1.25
520.063	80	47680.35	67.05	412.22	3.77	115.67	1.07
534.907	80	49316.20	75.71	442.67	4.14	111.41	1.05
549.35	80	50184.28	72.89	479.70	6.11	104.62	1.34
565.785	80	49313.24	52.73	508.13	4.33	97.05	0.83
581.735	80	47107.93	66.15	512.33	4.06	91.95	0.74
595.304	80	45029.56	66.13	526.09	6.40	85.59	1.05
609.711	80	43333.09	85.38	512.89	6.31	84.49	1.05
623.878	80	41609.48	62.51	487.79	4.14	85.30	0.74
640.77	80	40203.32	72.17	470.69	3.78	85.41	0.70
653.896	80	40208.45	49.01	446.42	6.39	90.07	1.29
667.462	80	38718.22	58.42	428.45	3.86	90.37	0.83
685.304	80	37349.45	46.66	417.03	3.42	89.56	0.74
699.608	80	36848.41	61.40	385.34	3.50	95.63	0.88
715.167	80	37227.91	68.96	382.15	3.86	97.42	1.00
730.678	80	36439.73	63.73	359.98	3.76	101.23	1.07
744.774	80	36075.26	61.81	357.82	3.16	100.82	0.91
761.137	80	35789.88	38.34	337.68	3.15	105.99	1.00
774.982	80	34935.76	64.14	331.44	3.15	105.40	1.02
789.042	80	34906.66	61.09	309.11	3.67	112.92	1.35
805.319	80	33163.83	64.53	286.92	2.59	115.59	1.07
817.762	80	32897.07	58.97	285.05	3.31	115.41	1.36
835.235	80	28963.01	40.30	249.45	2.81	116.11	1.32
851.054	80	27450.12	53.73	237.82	3.14	115.42	1.54
865.374	80	26156.75	44.35	220.52	3.31	118.61	1.79
881.45	80	26725.79	42.79	224.66	2.66	118.96	1.42
894.489	80	28635.35	37.22	242.21	3.31	118.23	1.62
910.163	80	32793.23	37.36	272.83	2.98	120.19	1.32
921.785	80	38754.52	41.75	329.94	3.15	117.46	1.13
938.896	80	47518.71	59.94	390.54	3.51	121.67	1.10
954.715	80	60004.85	43.64	502.59	5.26	119.39	1.25
965.181	80	81245.99	74.13	633.22	4.27	128.31	0.87
984.011	80	80176.48	89.60	555.01	3.63	144.46	0.96
999.777	80	56055.72	73.61	323.53	3.07	173.26	1.66
1025.74	80	60775.60	69.36	307.47	3.49	197.66	2.26
1046.17	80	183210.32	142.88	1071.04	5.40	171.06	0.87
1071.91	80	113290.98	103.05	569.68	5.08	198.87	1.78
1101.27	80	264081.82	182.50	1340.67	8.70	196.98	1.29
1122.46	80	99261.44	101.61	368.69	3.33	269.23	2.45
1143.56	80	89476.36	102.68	236.63	3.22	378.13	5.17
1172.55	80	91562.11	89.88	195.35	3.92	468.70	9.42
1195.81	80	102558.31	136.01	119.04	2.57	861.56	18.62
1235.39	80	157784.37	128.44	317.26	3.32	497.34	5.22
1276.18	80	271863.94	204.05	497.41	3.70	546.56	4.09

Figure C2: Laboratory data for NWA 7034. Units for ^{40}Ar and ^{39}Ar are in counts. The values reported here are the only ones used for analyses in this paper.

$J = 0.084099 \pm 0.0002523$

Temperature (˚C)	Step Duration (s)	Ar-40	Ar-40_Er	Ar-39	Ar-39_Er	Ar40/Ar39	Ar40/Ar39_Er
350	60	7.36E-02	1.43E-04	2.60E-03	3.72E-05	2.83E+01	5.50E-02
450	60	3.00E-01	2.54E-04	9.35E-03	7.15E-05	3.21E+01	2.72E-02
500	60	5.25E-01	2.74E-04	1.41E-02	7.28E-05	3.72E+01	1.94E-02
550	60	6.22E-01	3.02E-04	1.49E-02	5.71E-05	4.17E+01	2.03E-02
600	60	1.26E+00	4.86E-04	2.48E-02	6.96E-05	5.08E+01	1.96E-02
625	60	1.30E+00	4.87E-04	2.13E-02	6.18E-05	6.10E+01	2.29E-02
650	60	1.54E+00	5.55E-04	2.14E-02	7.35E-05	7.20E+01	2.59E-02
670	60	1.78E+00	6.24E-04	2.28E-02	9.83E-05	7.81E+01	2.74E-02
685	60	1.74E+00	5.63E-04	2.10E-02	6.13E-05	8.29E+01	2.68E-02
700	60	2.24E+00	1.06E-03	2.55E-02	6.20E-05	8.78E+01	4.16E-02
710	60	1.71E+00	6.59E-04	1.91E-02	5.36E-05	8.95E+01	3.45E-02
720	60	2.43E+00	6.25E-04	2.70E-02	6.89E-05	9.00E+01	2.31E-02
730	60	2.22E+00	5.67E-04	2.45E-02	6.36E-05	9.06E+01	2.31E-02
740	60	1.82E+00	7.88E-04	2.01E-02	6.85E-05	9.05E+01	3.92E-02
750	60	2.37E+00	8.94E-04	2.60E-02	7.30E-05	9.12E+01	3.44E-02
760	60	1.00E+00	3.77E-04	1.11E-02	4.82E-05	9.01E+01	3.40E-02
770	60	1.33E+00	5.00E-04	1.47E-02	5.02E-05	9.05E+01	3.40E-02
785	60	2.69E+00	7.69E-04	2.99E-02	1.36E-04	9.00E+01	2.57E-02
800	60	2.82E+00	9.17E-04	3.17E-02	9.53E-05	8.90E+01	2.89E-02
815	60	2.80E+00	1.10E-03	3.14E-02	7.38E-05	8.92E+01	3.50E-02
830	60	3.63E+00	1.34E-03	4.12E-02	1.09E-04	8.81E+01	3.25E-02
840	60	2.98E+00	1.43E-03	3.38E-02	8.16E-05	8.82E+01	4.23E-02
850	60	5.49E+00	2.09E-03	6.23E-02	9.92E-05	8.81E+01	3.35E-02
860	60	3.23E+00	1.19E-03	3.65E-02	8.69E-05	8.85E+01	3.26E-02
870	60	4.11E+00	1.06E-03	4.67E-02	1.01E-04	8.80E+01	2.27E-02
880	60	3.60E+00	9.87E-04	4.06E-02	1.06E-04	8.87E+01	2.43E-02
890	60	2.94E+00	7.77E-04	3.27E-02	7.51E-05	8.99E+01	2.38E-02
900	60	2.70E+00	6.80E-04	3.04E-02	7.12E-05	8.88E+01	2.24E-02
910	60	2.45E+00	6.40E-04	2.77E-02	7.05E-05	8.84E+01	2.31E-02
920	60	2.79E+00	7.24E-04	3.16E-02	8.55E-05	8.83E+01	2.29E-02
930	60	1.90E+00	5.96E-04	2.15E-02	6.17E-05	8.84E+01	2.77E-02
940	60	1.75E+00	5.35E-04	1.97E-02	6.91E-05	8.88E+01	2.72E-02
950	60	2.48E+00	7.37E-04	2.77E-02	7.13E-05	8.95E+01	2.66E-02
965	60	2.58E+00	9.68E-04	2.94E-02	7.12E-05	8.78E+01	3.29E-02
980	60	2.30E+00	5.64E-04	2.63E-02	7.12E-05	8.75E+01	2.14E-02
1000	60	2.12E+00	5.75E-04	2.44E-02	6.75E-05	8.69E+01	2.36E-02
1015	60	1.24E+00	4.79E-04	1.41E-02	4.89E-05	8.79E+01	3.40E-02
1035	60	1.69E+00	7.13E-04	1.97E-02	6.09E-05	8.58E+01	3.62E-02
1060	60	1.50E+00	5.72E-04	1.81E-02	8.00E-05	8.29E+01	3.16E-02
1080	60	8.79E-01	4.03E-04	1.21E-02	4.84E-05	7.26E+01	3.33E-02
1100	60	1.48E+00	4.70E-04	1.92E-02	5.50E-05	7.71E+01	2.45E-02
1130	60	2.53E+00	7.96E-04	3.31E-02	7.21E-05	7.64E+01	2.40E-02
1160	60	2.12E+00	5.87E-04	2.79E-02	8.33E+00	7.60E+01	2.10E-02
1190	60	3.34E+00	9.39E-04	4.26E-02	8.29E-05	7.84E+01	2.20E-02
1210	60	7.97E-01	3.63E-04	1.01E-02	5.77E-05	7.89E+01	3.59E-02
1250	60	3.41E-01	2.57E-04	4.06E-03	3.33E-05	8.40E+01	6.33E-02
1300	60	3.29E-01	2.69E-04	3.87E-03	3.80E-05	8.50E+01	6.95E-02

Figure C3: Laboratory data for 69945 from Norman et al. (2006). Units for ^{40}Ar and ^{39}Ar are in cc/g. The values reported here are the only ones used for analyses in this paper.